Mon. Not. R. Astron. Soc. **372,** 1093–1103 (2006) doi:10.1111/j.1365-2966.2006.10899.x

The scattering of Lyman-series photons in the intergalactic medium

Steven R. Furlanetto[1]★ and Jonathan R. Pritchard[2]

[1]*Yale Centre for Astronomy and Astrophysics, Yale University, PO Box 208121, New Haven, CT 06520-8121, USA*
[2]*California Institute of Technology, Mail Code 130-33, Pasadena, CA 91125, USA*

Accepted 2006 August 3. Received 2006 August 2; in original form 2006 May 25

ABSTRACT

We re-examine scattering of photons near the Lyα resonance in the intergalactic medium (IGM). We first derive a general integral solution for the radiation field around resonance within the usual Fokker–Planck approximation. Our solution shows explicitly that recoil and spin diffusivity source an absorption feature, whose magnitude increases with the relative importance of recoil compared to Doppler broadening. This spectrum depends on the Lyα line profile, but approximating it with the absorption profile appropriate to the Lorentzian wings of natural broadening accurately reproduces the results for a full Voigt profile so long as the IGM temperature is less than $\sim$1000 K. This approximation allows us to obtain simple analytic formulae for the total scattering rate of Lyα photons and the accompanying energy exchange rate. Our power series solutions converge rapidly for photons that redshift into the Lyα resonance as well as for photons injected at line centre. We confirm previous calculations showing that heating through this mechanism is quite slow and probably negligible compared to other sources. We then show that energy exchange during the scattering of higher-order Lyman-series photons can be much more important than naively predicted by recoil arguments. However, the resulting heating is still completely negligible.

Key words: line: profiles – radiative transfer – intergalactic medium.

1 INTRODUCTION

The radiative transfer of photons near the Lyα resonance is crucial to understanding the high-redshift intergalactic medium (IGM), both because it determines the spin temperature of the 21-cm transition (Wouthuysen 1952; Field 1958) and because it affects the thermal history (Madau, Meiksin & Rees 1997; Chen & Miralda-Escudé 2004).

The radiation field near this resonance has been examined a number of times in recent years. The earliest treatments ignored radiative transfer and assumed that the spectrum was featureless around the line. Chen & Miralda-Escudé (2004) were the first to solve (numerically) an approximate form of the radiative transfer equation in this context (following Basko 1981; Rybicki & dell'Antonio 1994). They showed that, if photons redshift towards the resonance, the spectrum develops an asymmetric absorption feature. As we will see explicitly below, the absorption feature is sourced by recoil in the scattering process: each scattering deposits an average energy $\Delta E = (h\nu_\alpha)^2/(m_{\rm p}c^2)$, where ν_α is the rest frequency of the Lyα line. Thus photons lose energy faster near the centre of resonance, where they scatter more. To compensate for this increased 'flow' speed, continuity requires that the amplitude of the background must decrease near resonance. This affects the scattering rate of Lyα photons and hence the spin temperature of the IGM. Hirata (2006) expanded on this method by showing how to account for the hyperfine structure of the Lyα line (see below).

An alternative to the numerical approach of Chen & Miralda-Escudé (2004) and Hirata (2006) is to approximate the spectrum analytically. This has a long history in resonant radiative transfer; Hummer & Rybicki (1992) summarized many of the advances. Of particular interest to our problem is the treatment of Grachev (1989), who derived an analytic solution for the spectrum around a resonant transition when recoil is included. The analytic solution was obtained by approximating the absorption profile using the form appropriate for scattering in the Lorentzian wings provided by natural broadening. This assumption is valid when the optical depth is extremely large and the Doppler broadening relatively small. Most recently, Chuzhoy & Shapiro (2006a) rediscovered this solution and applied it to the problem of Lyα transfer in the high-redshift IGM. In Section 2, we will show how these numeric and analytic solutions relate and study the validity of the analytic approximation. We also compute the radiation field in such a way that the role of recoil becomes obvious. We examine the resulting total scattering rate in Section 3 and show that the approximate form proposed by Chuzhoy & Shapiro (2006a) is a reasonably good match to the full numeric result. We also compute the colour temperature of the radiation field (relevant for the spin temperature of the 21-cm transition) in Section 4.

The line shape is also crucial for estimating the rate at which energy is transferred between the gas and the photon field. As described above, recoil during each scattering deposits some energy in the gas.

★E-mail: steven.furlanetto@yale.edu

If this were the sole mechanism for energy exchange, the IGM would rapidly be heated above the cosmic microwave background (CMB) temperature (Madau et al. 1997). However, the absorption feature actually cancels almost all of this heating. Consider a photon on the blue side of the line. This will be preferentially scattered by an atom moving *away* from the photon (so that it appears closer to resonance). The atom will then re-emit the photon isotropically in its frame; in the IGM frame, the photon will therefore lose an energy $\sim h\Delta\nu_{\rm D}$, where $\Delta\nu_{\rm D}$ is the Doppler width of the transition. Photons that scatter on the red side, on the other hand, will tend to gain energy. The absorption feature develops so that this scattering 'diffusivity' compensates for the recoil (i.e. so that more scattering occurs redward than blueward of the Lyα transition). The net energy transfer is therefore much slower than naively expected (Chen & Miralda-Escudé 2004; Meiksin 2006; Rybicki 2006).

By employing their analytic approximation to the radiation field, Chuzhoy & Shapiro (2006b) took a step towards finding a simple solution for the net heating rate. In Section 5, we take their approach further by deriving a fully analytic solution for heating by photons redshifting into the Lyα resonance as well as an approximate solution for photons injected at line centre (either through recombinations or through cascades from higher Lyn transitions). This allows us to examine how the heating rate varies with IGM temperature and optical depth.

Of course, photons can redshift into any of the Lyn resonances in the IGM. After a few scatterings, these photons are destroyed through cascades to lower levels (Hirata 2006; Pritchard & Furlanetto 2006). The scattering rate is so small that recoil heating is negligible; however, all of the scatterings occur on the blue side of the line, so each deposits some fraction of the atom's thermal energy in the gas as well. Chuzhoy & Shapiro (2006b) examined the analogous process in deuterium and found that it can provide relatively strong heating. In Section 6, we show that the heating rate for Lyn photons is tiny even when frequency drift is included, because the photons scatter so far in the blue wing of the line.

In our numerical calculations, we assume a cosmology with $\Omega_{\rm m} = 0.26$, $\Omega_\Lambda = 0.74$, $\Omega_{\rm b} = 0.044$ and $H = 100\,h\,{\rm km\,s^{-1}\,Mpc^{-1}}$ (with $h = 0.74$), consistent with the most recent measurements (Spergel et al. 2006).

2 THE RADIATION FIELD NEAR THE Lyα RESONANCE

We let J be the comoving angle-averaged specific intensity (in units of photons per area per steradian). The equation of radiative transfer is (neglecting atomic recoil for the moment)

$$\frac{1}{cn_{\rm H}\chi_\alpha}\frac{\partial J}{\partial t} = -\phi(\nu)\,J + H\nu_\alpha\frac{\partial J}{\partial \nu} + \int {\rm d}\nu'\,R(\nu,\nu')\,J(\nu') + C(t)\psi(\nu), \quad (1)$$

where $n_{\rm H}$ is the hydrogen density, $\sigma_\alpha(\nu) = \chi_\alpha\phi(\nu)$ is the absorption cross-section, $\chi_\alpha = (\pi e^2/m_{\rm e}c)\,f_\alpha$, f_α is the absorption oscillator strength and $\phi(\nu)$ is the line profile. For our purposes, ϕ is given by the Voigt profile (which includes both collisional and natural broadening),

$$\phi(x) = \frac{a}{\pi^{3/2}}\int_{-\infty}^{\infty}{\rm d}t\,\frac{{\rm e}^{-t^2}}{a^2+(x-t)^2}, \quad (2)$$

with $a = \Gamma/(4\pi\Delta\nu_{\rm D})$, Γ the inverse lifetime of the upper state, $\Delta\nu_{\rm D}/\nu_0 = (2k_{\rm B}T_{\rm K}/mc^2)^{1/2}$ the Doppler parameter, ν_0 the line centre frequency, $T_{\rm K}$ the gas temperature, and $x \equiv (\nu-\nu_0)/\Delta\nu_{\rm D}$ the normalized frequency shift. The first term on the right-hand side of equation (1) describes absorption, the second the Hubble flow, and the third re-emission following absorption. The redistribution function $R(\nu,\nu')$ gives the probability that a photon absorbed at frequency ν' is re-emitted at frequency ν. The approximate form $R_{\rm II}(\nu,\nu')$ (Henyey 1941; Hummer 1962), which assumes a Voigt profile with coherent scattering in the rest frame of the absorbing atom, is often used (see Section 6). We must, however, also include recoil (Basko 1981) and, for exact calculations, spin exchange (Hirata 2006; Chuzhoy & Shapiro 2006a). The last term describes injection of new photons: C is the rate at which they are produced and $\psi(\nu)$ is their frequency distribution.

This integrodifferential equation simplifies considerably if we assume that the background spectrum is smooth on the scale of the average frequency change per scattering (which is $\Delta x < 1$; see Section 6). In this Fokker–Planck approximation, equation (1) becomes (Rybicki & dell'Antonio 1994)

$$\frac{\rm d}{{\rm d}x}\left\{\phi(x)\frac{{\rm d}J}{{\rm d}x} + 2[\eta'\phi(x)+\gamma']J(x)\right\} + C\psi(x) = 0. \quad (3)$$

The coefficients γ' and η' depend on the scattering processes that are included in the redistribution function. Inserting the Hubble flow, recoil, and spin exchange, and further assuming that $x \gg \nu_{21}/\Delta\nu_{\rm D}$ (where ν_{21} is the frequency of the hyperfine transition),[1] these become (Chuzhoy & Shapiro 2006a; Hirata 2006)

$$\gamma' = \tau_{\rm GP}^{-1}\left(1+\frac{T_{\rm se}}{T_{\rm K}}\right)^{-1}, \quad (4)$$

$$\eta' = \eta\left(\frac{1+T_{\rm se}/T_{\rm S}}{1+T_{\rm se}/T_{\rm K}}\right) - (x+x_0)^{-1}, \quad (5)$$

where $\tau_{\rm GP}$ is the total Gunn & Peterson (1965) optical depth of the Lyα transition, $\eta = (h\nu_0^2)/(mc^2\Delta\nu_{\rm D})$ is the mean (normalized) frequency drift per scattering from recoil (Basko 1981), $x_0 \equiv \nu_0/\Delta\nu_{\rm D}$ (this term enforces detailed balance; Rybicki 2006), $T_{\rm S}$ is the spin temperature of the 21-cm transition, and $T_{\rm se} = (2/9)T_{\rm K}\nu_{21}^2/\Delta\nu_{\rm D}^2 = 0.40\,{\rm K}$. Before proceeding, we must note that equation (3) is not uniquely specified because there is some freedom in the drift and diffusivity imposed in the Fokker–Planck method. Other forms of the Fokker–Planck approximation have been examined by Meiksin (2006). Its utility for this problem has been verified numerically in some particular cases by Hirata (2006), but its accuracy for the general problem has not yet been fully explored (see also Meiksin 2006). We discuss its validity in more detail in Section 7.

The corrections for spin exchange, which are captured by the terms involving $T_{\rm se}$, require some subtlety. Because Lyα transitions modify the ground-state hyperfine level populations (Wouthuysen 1952; Field 1958), the photons can also increase or decrease their frequency during each scattering by an amount corresponding to the energy defect of the 21-cm transition. This affects the flow rate of photons through the resonance (and the diffusivity) and hence the spectral shape. However, because the level populations themselves depend on the Lyα scattering rate, and because the mean energy exchange per scattering depends on the level populations, including spin exchange requires a simultaneous solution for $T_{\rm S}$ and the spectral shape (or, in practice, an iterative solution; Hirata 2006). For simplicity, we will neglect these corrections below. For clarity, we will therefore use $\gamma = \tau_{\rm GP}^{-1}$ and η instead of their primed

[1] When $x \sim \nu_{21}/\Delta\nu_{\rm D}$, the hyperfine splitting of the Lyα line cannot be ignored and a single line profile does not suffice; see Hirata (2006).

versions. To include spin exchange, one simply reverses this, as in Furlanetto, Oh & Briggs (2006) or Hirata (2006). The latter also shows the magnitude of these corrections (his fig. 2): they are only a few per cent except at $T_{\rm K} \lesssim 1$ K (see also the discussion in Section 7, below).[2]

It is useful now to pause and note explicitly the scalings of the basic parameters of this problem; they will become useful later. We have $\Delta\nu_{\rm D} \propto T_{\rm K}^{1/2}$, so $a \propto T_{\rm K}^{-1/2}$ and $\eta \propto T_{\rm K}^{-1/2}$. The Sobolev parameter has $\gamma \propto (1+z)^{-3/2}$ in the high-redshift limit. Of course, spin exchange slightly modifies these scalings.

We will consider two sets of boundary conditions for equation (3). First, we let photons redshift into the resonance from large frequencies, with no injection term. To describe this we let $J_\infty > 0$ be the specific intensity as $x \to \infty$ and set $C = 0$. The second case allows injection at line centre, so $C\psi(x) = C\delta(x)$,[3] and sets $J_\infty = 0$. In this case, we define $J_{-\infty}$ to be the average intensity as $x \to -\infty$. In either scenario, equation (3) is easy to integrate once, leaving us with a first-order ordinary differential equation. The formal solution is most transparently obtained by changing variables to (Hummer & Rybicki 1992)

$$\sigma(x) = \int_0^x \frac{{\rm d}x'}{\phi(x')}, \tag{6}$$

so that equation (3) becomes

$$\frac{{\rm d}J}{{\rm d}\sigma} + 2(\eta\phi + \gamma)J = 2K, \tag{7}$$

where $K = \gamma J_\infty$ for the continuous case, $K = C$ for injected photons if $x < 0$, and $K = 0$ for injected photons with $x > 0$. Obviously

$$\exp\left[2\eta \int_0^\sigma \phi(\sigma'){\rm d}\sigma' + 2\gamma\sigma\right] \tag{8}$$

is an integrating factor for this equation, from which the solution follows immediately. For injected photons with $x > 0$ (so that $K = 0$), it has the simple form

$$J(x) = J(0)\exp\left[-2\eta x - 2\gamma \int_0^x \frac{{\rm d}x'}{\phi(x')}\right], \tag{9}$$

where $J(0)$ is determined by continuity.

A formal solution can also be written for $K > 0$, but in this case an alternate form is more physically illuminating. Here it is the absorption trough that is most interesting. To isolate its properties, we define $\delta_J \equiv (J_\infty - J)/J_\infty$;[4] note then that $\delta_J > 0$. The transfer equation takes the form

$$\phi\frac{{\rm d}\delta_J}{{\rm d}x} + 2(\eta\phi + \gamma)\delta_J = 2\eta\phi. \tag{10}$$

This has the same structure as the previous version, except that the sourcing term on the right-hand side depends on x. The same integrating factor yields the solution

$$\delta_J(x) = 2\eta \int_0^\infty {\rm d}y \exp\left[-2\eta y - 2\gamma \int_{x-y}^x \frac{{\rm d}x'}{\phi(x')}\right]. \tag{11}$$

[2] Note that our definition of S_α below corresponds to $\tilde{S}_\alpha$ in Hirata (2006): see Section 4.

[3] Even if the initial Lyman-series absorption occurs well blueward of line centre, the Lyα photon that results from the cascade will be injected near line centre because the atom passes through several intermediate states, each of which has a small natural width.

[4] For injected photons, $J_\infty = 0$, of course; then we make the substitution $J_\infty \to J_{-\infty}$ in the definition. We will see that $J_\infty = J_{-\infty}$ for a redshifting continuum.

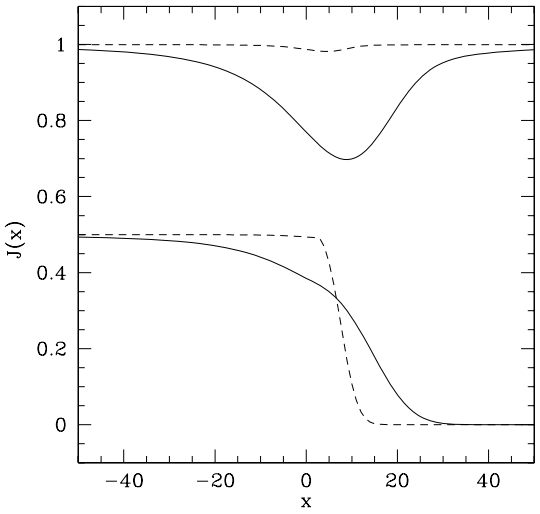

Figure 1. Background radiation field near the Lyα resonance at $z = 10$, assuming a Voigt line profile. The upper and lower sets are for photons redshifting from infinity and photons injected at line centre, respectively. (The former are normalized to J_∞; the latter have $J_{-\infty} = 1/2$.) The solid and dashed curves take $T_{\rm K} = 10$ and 1000 K, respectively.

This form makes it obvious that recoil sources the absorption spike. If the scattering were purely coherent, the gas and radiation field could not transfer any energy and the spectrum would remain flat (see e.g. Hummer & Rybicki 1992). By sapping energy from each scattered photon, recoil increases the rate at which they redshift across the resonance. This increase in the 'flow velocity' must be balanced by a corresponding decrease in the photon flux near the resonance.

We show some example spectra in Fig. 1, assuming that $\phi(x)$ has a Voigt profile (see also Chen & Miralda-Escudé 2004). The upper curves assume that photons redshift into resonance from infinity; as expected, an absorption feature develops. It deepens at small temperatures, because, in that case, the energy lost from recoil is large compared to the energy lost in each scattering (or η is relatively large). The lower curves assume injection at line centre. In this case, the spectrum spreads to large positive x when $T_{\rm K}$ decreases.

This numerical solution is, of course, identical to those presented by Chen & Miralda-Escudé (2004) and Hirata (2006), once the appropriate line profiles, drifts and diffusivities are inserted. It is also a more general form of the solutions provided by Hummer & Rybicki (1992) (who neglected the recoil term) and Chuzhoy & Shapiro (2006a). The latter implicitly made the approximation (following Chugai 1980, 1987; Grachev 1989) that $\phi(x) \approx a/(\pi x^2)$, which is only accurate at $|x| \gg 1$. We will refer to this as the 'wing' approximation for convenience. This approximation allows the integrals over ϕ^{-1} to be performed analytically (Grachev 1989; Chuzhoy & Shapiro 2006a). For injected photons with $x > 0$, the solution is

$$J(x) = J(0)\exp\left(-2\eta x - \frac{2\pi}{3}\frac{\gamma x^3}{a}\right), \tag{12}$$

while for a flat background or injected photons with $x < 0$,

$$\delta_J(x) = 2\eta \int_0^\infty {\rm d}y \exp\left[-\frac{2\pi\gamma}{3a}(y^3 - 3y^2x + 3yx^2) - 2\eta y\right]. \tag{13}$$

This explains the discrepancy between the existing numeric and analytic results: the latter do not apply near the Doppler core of the profile.

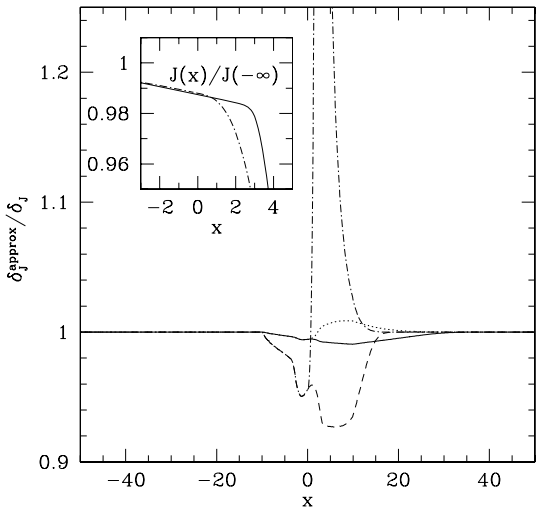

Figure 2. Ratio of δ_J in the 'wing' approximation to the exact results (using a Voigt profile). The solid and dashed curves assume a flat background spectrum and take $T_K = 10$ and 1000 K, respectively. The dotted and dot–dashed curves assume injection at line centre, with $T_K = 10$ and 1000 K, respectively. In this case, we set $\delta_J = J/J_{-\infty}$ for $x > 0$. The inset shows a close-up of J near resonance for injected photons at $T_K = 1000$ K; the solid and dot–dashed curves show the exact and approximate solutions, respectively. All curves assume $z = 10$.

Fig. 2 shows the ratio of the approximate analytic solutions of Grachev (1989) and Chuzhoy & Shapiro (2006a) to the exact spectra (computed with a Voigt profile).[5] When the temperature is small (solid and dotted curves), the approximation is an excellent one. However, it begins to break down at large temperatures: for example, in the continuous case with $T_K = 1000$ K, it underpredicts δ_J by $\sim$10 per cent at the centre of the absorption spike. This is because the effective natural width decreases with temperature, so the thermal broadening becomes more important in higher-temperature gas. Note as well that the deviation has a non-trivial shape. This is because the character of the wing approximation changes depending on whether x is less than or greater than unity (that is, $\phi \to \infty$ when $x \to 0$ in the wing approximation). The deviation is worst for injected photons, especially at high temperatures. The physical effects are still small, however; in the inset we show a close-up of the spectrum itself near $x = 0$. We see that, in the wing approximation, the decline at $x > 0$ occurs a bit earlier. The fractional deviation is therefore large, but only over a limited range of frequencies (and only outside the line core).

Overall, we find that the wing approximation is an excellent one. Below we will use this analytic form to study the scattering and heating rates, extending the approach of Chuzhoy & Shapiro (2006a,b).

3 THE Lyα SCATTERING RATE

The total rate at which Lyα photons scatter (per hydrogen atom) is

$$P_\alpha = 4\pi\chi_\alpha \int_{-\infty}^{\infty} \mathrm{d}\nu\, J(\nu)\phi(\nu), \tag{14}$$

where J is now in proper units. Because each scattering can exchange hyperfine states, this rate is crucial for determining the spin temperature of the 21-cm transition in the IGM (Wouthuysen 1952; Field 1958; Madau et al. 1997; Chen & Miralda-Escudé 2004; Chuzhoy & Shapiro 2006a; Hirata 2006). The Wouthuysen–Field coupling strength can be written as (e.g. Furlanetto et al. 2006)[6]

$$x_\alpha = \frac{16\pi\chi_\alpha J_\infty}{27A_{10}} \frac{T_\star}{T_\gamma} S_\alpha, \tag{15}$$

where $A_{10} = 2.85 \times 10^{-15}\ \mathrm{s}^{-1}$ is the spontaneous emission coefficient of the 21-cm transition, $T_\star = 0.068$ K is the energy defect of that transition, T_γ is the CMB temperature and

$$S_\alpha \equiv \int_{-\infty}^{\infty} \mathrm{d}x\, \phi(x) \frac{J}{J_\infty} \tag{16}$$

depends only on the *shape* of the background spectrum. Note that $S_\alpha < 1$, because recoil always induces an absorption feature.

In general, S_α must be computed numerically; even in the wing approximation, there is no closed-form analytic solution. However, recall that $\phi(x)$ is sharply peaked around $x = 0$, while J varies slowly near resonance (even in the injected case). Thus we can approximate $J \approx J(0)$ everywhere inside the integral; from the normalization of ϕ we thus have

$$1 - S_\alpha \approx \delta_J(0). \tag{17}$$

In the wing approximation, this is easily computed from equation (13):

$$1 - S_\alpha \approx \frac{4\alpha}{9}\left[3^{2/3}\pi \mathrm{Bi}\left(-\frac{2\alpha}{3^{1/3}}\right) + (3\alpha^2)\,{}_1F_2\left(1; \frac{4}{3}, \frac{5}{3}; -\frac{8\alpha^3}{27}\right)\right], \tag{18}$$

$$\approx \frac{4\pi}{3\sqrt{3}\Gamma(2/3)}\alpha - \frac{8\pi}{3\sqrt{3}\Gamma(1/3)}\alpha^2 + \frac{4}{3}\alpha^3 + \cdots, \tag{19}$$

where Bi (x) is an Airy function, ${}_1F_2$ is a hypergeometric function, and

$$\alpha = \eta\left(\frac{3a}{2\pi\gamma}\right)^{1/3} = 0.717 T_K^{-2/3}\left(\frac{10^{-6}}{\gamma}\right)^{1/3}, \tag{20}$$

where T_K is in Kelvin; note that the second equality is not exact when spin exchange is important (which requires the replacements $\gamma \to \gamma'$ and $\eta \to \eta'$) or when the correction for detailed balance is significant. When α is small, we therefore have $(1 - S_\alpha) \propto T_K^{-2/3}\tau_{GP}^{1/3}$. This scaling gives some intuition for how the coupling strength varies in the IGM. As in Fig. 1, the absorption spike becomes less and less significant as T_K increases; thus we must have $S_\alpha \to 1$ (its value without recoil) in a warm IGM. The perturbation increases with optical depth because that increases the number of scatterings (and hence the energy loss due to recoil).

We show the dependence of $(1 - S_\alpha)$ on temperature in Fig. 3 and the dependence on the Sobolev parameter (or optical depth) in Fig. 4. The thick curves show the numeric solution for a Voigt line profile and for a continuous background spectrum, which we denote S_c. The case with photons injected at the line centre has a nearly identical scattering integral, because $\delta_J(0)$ is the same in the two cases; only at high temperatures does the structure around resonance matter. The thin curves show the first-order (in α) approximation of equation (19). We see that this provides an excellent match at $T_K \gtrsim 10$ K, especially when γ is relatively large (i.e. at lower redshifts).

[5] Or, more precisely, the exact solution within the Fokker–Planck approximation.

[6] For injected photons, one must substitute $J_\infty \to J_{-\infty}$. Note as well that J_∞ must be in proper units.

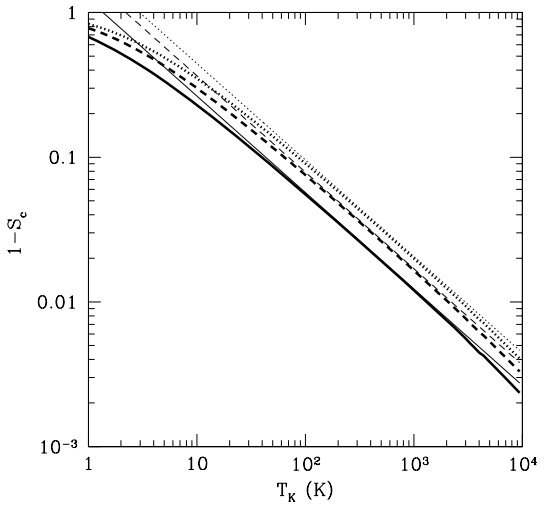

Figure 3. Scattering integral as a function of IGM temperature. The thick solid, dashed and dotted curves show $(1 - S_c)$ for a Voigt profile at $z = 10, 20$ and 30. The thin curves show the corresponding quantities using only the first-order term in equation (19).

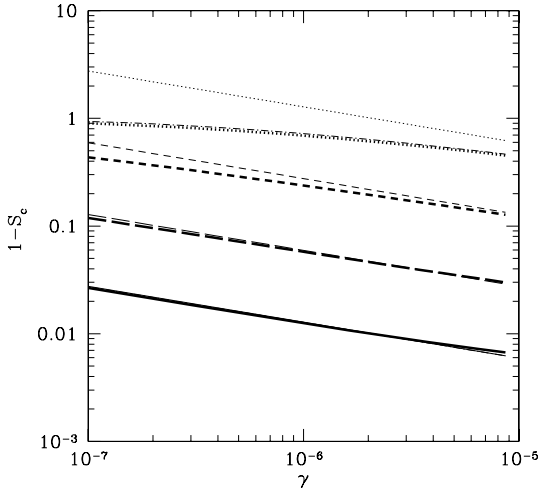

Figure 4. Scattering integral as a function of $\gamma = \tau_{\rm GP}^{-1}$. The thick curves show $(1 - S_c)$ computed numerically for a Voigt profile, while the thin curves show the corresponding quantities using only the first-order term in equation (19). The dotted, short-dashed, long-dashed and solid curves take $T_K = 1, 10, 10^2$ and 10^3 K, respectively. The thin dot–dashed curve shows the approximate form proposed by Chuzhoy & Shapiro (2006a) for $T_K = 1$ K.

Note that we have actually made three approximations here: (i) a constant J across the line; (ii) the wing approximation and (iii) the small α approximation. The culprit at small T_K is the third. Here α is large and the power series approximation breaks down. However, even including just terms up to α^3 dramatically improves the estimate, with errors $\lesssim$10 per cent so long as $T_K > 2$ K. This demonstrates that the first approximation is an excellent one here: at such small temperatures, $\phi(x)$ is extremely sharply peaked. The second is equally good. Chuzhoy & Shapiro (2006a) proposed the fit

$$\delta_J(0) \approx 1 - \exp(-1.79\alpha), \tag{21}$$

which retains the first-order behaviour of $\delta_J(0)$ at small α (and hence is reasonably accurate) and fits the behaviour for $\alpha \sim 1$ much better. The thin dot–dashed curve in Fig. 4 shows how well this approximation does at $T_K = 1$ K; it typically differs from the exact solution by $\sim$5 per cent.

The overall agreement worsens at large temperatures as well. Here α is small, so the power series in equation (19) converges rapidly and approximation (iii) is excellent. The problem lies instead with the other two. As we have seen, the wing approximation breaks down once T_K exceeds $\sim$1000 K. This causes up to a 10 per cent underestimate of $\delta_J(0)$. At the same time, approximation (i) breaks down and the region around resonance starts to contribute to the scattering integral. This causes a $\lesssim$20 per cent overestimate of $(1 - S_c)$ compared to the exact result; fortunately, these two effects partially cancel.

In summary, the fit proposed by Chuzhoy & Shapiro (2006a) (in equation 21) is an excellent approximation (within the Fokker–Planck formalism) to S_α unless high accuracy is required. However, we emphasize that, in order to include spin exchange properly, one must still use an iterative procedure (Hirata 2006).

4 THE COLOUR TEMPERATURE

The Lyα radiation field couples the spin temperature T_S to an effective colour temperature T_c, defined as (Rybicki 2006)

$$\frac{h}{k_B T_c} \equiv -\frac{{\rm d}\ln n_\nu}{{\rm d}\nu}, \tag{22}$$

where $n_\nu = c^2 J/2\nu^2$ is the photon occupation number. The spin temperature is then determined by (Field 1958; Madau et al. 1997)

$$T_S^{-1} = \frac{T_\gamma^{-1} + x_c T_K^{-1} + x_\alpha T_c^{-1}}{1 + x_c + x_\alpha}, \tag{23}$$

where T_γ is the CMB temperature and x_c is the collisional coupling coefficient (see Furlanetto et al. 2006, and references therein). Of course, because of the non-trivial spectral shape near the Lyα resonance, T_c is actually a function of frequency; it should be harmonically averaged across the line profile to compute the effective coupling temperature (Chen & Miralda-Escudé 2004; Meiksin 2006). However, that makes only a small difference because the spectrum is so smooth (for the same reasons that equation 17 is a good approximation).

At resonance, we can solve equation (3), with spin exchange included, to obtain (for photons that redshift into resonance)

$$\frac{h}{k_B T_c} = \frac{2\eta'}{\Delta\nu_D} - \frac{2\gamma'}{\phi_0 \Delta\nu_D}\,\frac{J_\infty - J}{J}, \tag{24}$$

where the 0 subscript indicates evaluation at $x = 0$. The second term describes the deviation sourced by the Hubble flow. It is generally small (and formally vanishes in the wing approximation) but is easily included; the result is (Chuzhoy & Shapiro 2006a)

$$T_c = T_K \left[\left(\frac{1 + T_{se}/T_S}{1 + T_{se}/T_K} \right) - \frac{\gamma'}{\eta\phi_0}\,\frac{\delta_{J,0}}{1 + \delta_{J,0}} \right]^{-1}. \tag{25}$$

Ignoring the Hubble flow term, this matches the fit to numeric results proposed by Hirata (2006), provided that the correction from spin exchange is small. The Hubble flow term vanishes at small temperatures because then $\eta \gg \gamma'$; it also vanishes at high temperatures because then $\delta_{J,0}$ is small. It is never greater than $\sim 10^{-4}$. The spin exchange correction can be much larger.

Note that, because T_c itself depends on T_S, equation (23) is an implicit equation for the spin temperature and must usually be solved simultaneously with the spectral shape and scattering rate. However, when $T_K, T_S \gg 1$ K, the corrections are small (Hirata 2006).

5 HEAT EXCHANGE FROM Lyα SCATTERING

5.1 Continuous background

The rate at which the radiation field deposits energy in the gas (per unit volume) is (Chen & Miralda-Escudé 2004)

$$\epsilon_\alpha = \frac{4\pi H h \nu_0}{c} \int_{-\infty}^{\infty} \mathrm{d}\nu\, (J_\infty - J), \tag{26}$$

where we have assumed $\nu \approx \nu_0$ across the absorption feature and J is again in proper units. The physical interpretation of this form is straightforward: in the absence of scattering, the absorption feature would redshift away to infinity. To keep it in place, the photons must lose energy at the rate given in equation (26). More formally, it can be derived from the average energy exchange per scattering (Chuzhoy & Shapiro 2006b) through integration by parts and the use of equation (3).

Thus the heating rate depends on

$$I_\mathrm{c} = \int_{-\infty}^{\infty} \mathrm{d}x\, \delta_J(x), \tag{27}$$

$$= 2\eta \int_0^\infty \mathrm{d}y\, \mathrm{e}^{-2\eta y} \int_{-\infty}^{\infty} \mathrm{d}x \exp\left[-2\gamma \int_{x-y}^{x} \frac{\mathrm{d}x'}{\phi(x')}\right]. \tag{28}$$

This cannot be done in closed form for an arbitrary line profile, but the accuracy of the wing approximation makes it extremely useful in understanding the solution.[7] In this case, both integrals can be done analytically, yielding

$$I_\mathrm{c} = \left(\frac{4}{\pi}\right)^{-1/6} \pi^{3/2} \left(\frac{a}{\gamma}\right)^{1/3} \beta \left[\mathrm{Ai}^2(-\beta) + \mathrm{Bi}^2(-\beta)\right], \tag{29}$$

where

$$\beta = \eta \left(\frac{4a}{\pi\gamma}\right)^{1/3} = 0.99 T_\mathrm{K}^{-2/3} \left(\frac{\gamma^{-1}}{10^6}\right)^{1/3}, \tag{30}$$

and $\mathrm{Ai}(x)$ and $\mathrm{Bi}(x)$ are the Airy functions and T_K is in Kelvin. Note that this solution is *exact* within the wing approximation (although including spin exchange requires $\gamma \to \gamma'$ and $\eta \to \eta'$, so the second equality in equation 30 is only approximate; it also ignores the detailed balance correction).

We can again find a simple and useful approximation by expanding in powers of β. We find

$$I_\mathrm{c} \approx 3^{1/3} \left(\frac{2\pi}{3}\right)^{5/3} \left(\frac{a}{\gamma}\right)^{1/3} \left[\frac{\beta}{\Gamma^2(2/3)} - \frac{3^{1/3}\beta^2}{\Gamma(1/3)\Gamma(2/3)} + \frac{3^{2/3}\beta^3}{\Gamma^2(1/3)} + \ldots\right]. \tag{31}$$

Thus, we see $I_\mathrm{c} \propto T_\mathrm{K}^{-5/6}\, \gamma^{-2/3}$; because $\gamma = \tau_\mathrm{GP}^{-1} \propto (1+z)^{-3/2}$ at high redshifts, we expect $I_\mathrm{c} \propto (1+z)$ at fixed temperature. The heat input per atom per Hubble time (at constant J_∞) is therefore $\Delta T \propto H \Delta\nu_\mathrm{D} I_\mathrm{c}/(n_\mathrm{H_I} H) \propto T_\mathrm{K}^{-1/3}(1+z)^{-2}$. These scalings are close to those estimated by Chuzhoy & Shapiro (2006b) from their numerical results.

We show our solution for I_c as a function of T_K in the left-hand panel of Fig. 5 and as a function of γ in Fig. 6. In each of these panels, the thick curves use the full Voigt profile, while the thin curves use the first-order term (in β) of equation (31); we expect the latter to be valid when $T_\mathrm{K} \gtrsim 100\,\mathrm{K}$. The right-hand panel of Fig. 5 shows the ratio of the approximate and exact solutions; here the thick curves retain only the lowest order term, while the thin curves include terms up to β^3: these are necessary for $T_\mathrm{K} \lesssim 10\,\mathrm{K}$. As before, the expansion in equation (31) converges rapidly at higher temperatures, but the wing approximation begins to break down.

Obviously the predicted scalings are reasonably accurate; the heating rate decreases with temperature (because recoil becomes relatively inefficient) and increases with τ_GP (along with the scattering rate). The higher-order terms, and the Voigt profile, slightly decrease the dependence on these parameters. As shown by Chen & Miralda-Escudé (2004), Lyα heating is probably slow compared to other processes, and the wing approximation (in the full analytic expression for small temperatures and the power series form otherwise) should be adequate for most purposes.

5.2 Injection at line centre

For photons injected at the line centre, a similar exercise shows that the relevant integral is (Chen & Miralda-Escudé 2004)

$$I_i = \int_{-\infty}^{0} \mathrm{d}x\, \delta_J(x) - \int_0^\infty \mathrm{d}x\, \frac{J(x)}{J_{-\infty}}. \tag{32}$$

Again, we work in the wing approximation to gain some intuition. The second integral can be written in closed form; the first is

$$\int_{-\infty}^{0} \mathrm{d}x\, \delta_J = \frac{\eta}{\sqrt{2}} \sqrt{\frac{a}{\gamma}} \int_0^\infty \frac{\mathrm{d}y}{\sqrt{y}} \exp\left(-\frac{\pi\gamma}{6a} y^3 - 2\eta y\right) \times \mathrm{erfc}\left(\sqrt{\frac{\pi\gamma}{2a}} y^3\right). \tag{33}$$

Unfortunately, the complementary error function prevents a closed form solution. However, note that the exponential term implies that the integral is dominated by the region where the argument of the error function is small. Expanding it to lowest order, we then obtain a power series solution in β:

$$I_i \approx \left(\frac{a}{\gamma}\right)^{1/3} \sum_{i=0}^{\infty} A_i \beta^i. \tag{34}$$

The first few terms have $(A_0, A_1, A_2) = (-0.6979, 2.5424, -2.5645)$. Retaining only the zeroth-order term, the scaling with γ and T_K is again close to that proposed by Chuzhoy & Shapiro (2006b) at $T_\mathrm{K} \gtrsim 100\,\mathrm{K}$.

Figs 7 and 8 show I_i for the same parameters as in Figs 5 and 6; again we compare the approximate form with the exact solution (including the full Voigt profile). In this case the dependence on both T_K and γ is considerably more complicated. Most interestingly, injected photons can both heat the gas (when $T_\mathrm{K} \lesssim 10\,\mathrm{K}$) and cool it. Physically, cooling can occur because more photons scatter on the red than the blue side of the line; in such events, the re-emitted photon generally has a higher energy in the IGM frame and so removes heat from the gas. In the high-temperature regime ($T_\mathrm{K} \gtrsim 100\,\mathrm{K}$), the cooling rate falls slightly when γ decreases and when T_K increases. At small temperatures, the exchange switches to heating because the feature is so broad compared to the $\Delta x \sim 1$ frequency change per scattering.

We also show the approximate form (equation 34) in these panels (note that we must include β^0 and β^1 terms). It is substantially less accurate at first order in β, only approaching the exact solution at $T_\mathrm{K} \gtrsim 200\,\mathrm{K}$; shortly thereafter, the Voigt profile becomes significant. However, the thin curves in the right-hand panel of Fig. 8 show

[7] Note that Chuzhoy & Shapiro (2006b) calculated the heating rate numerically both in the wing approximation and using the full Voigt profile.

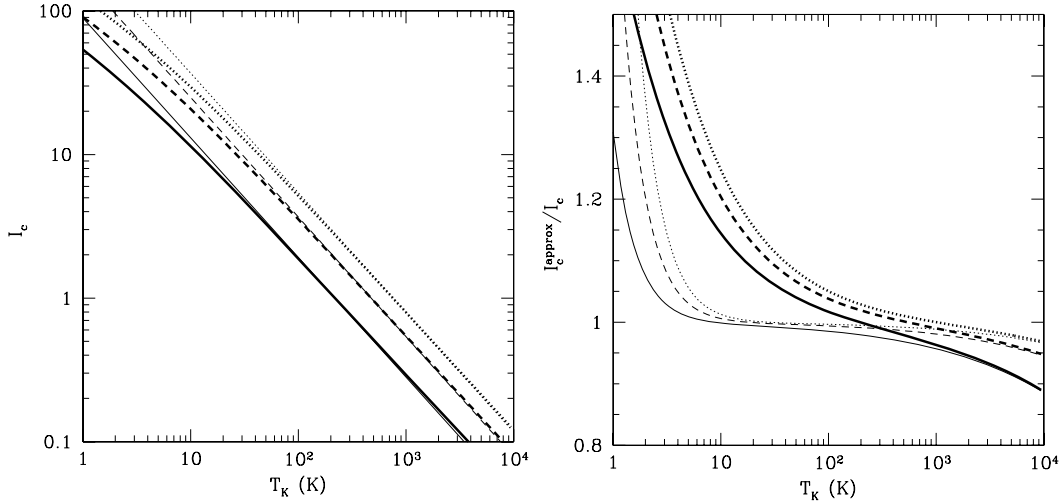

Figure 5. Heating integral for continuous injection. Left-hand panel: the thick solid, dashed and dotted curves show I_c for a Voigt profile at $z = 10, 20$ and 30. The thin curves show the corresponding quantities using only the first-order term in equation (31). Right-hand panel: ratio of the power series approximation to I_c (using the wing approximation) to the exact value. The thick and thin curves retain terms to order β and β^3, respectively.

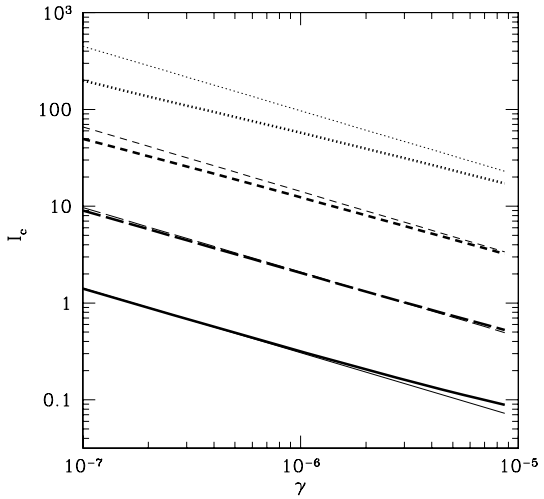

Figure 6. Heating integral for continuous injection. The thick curves show I_c computed numerically for a Voigt profile, while the thin curves show the corresponding quantities using only the first-order term in equation (31). The dotted, short-dashed, long-dashed and solid curves take $T_K = 1, 10, 10^2$ and 10^3 K, respectively.

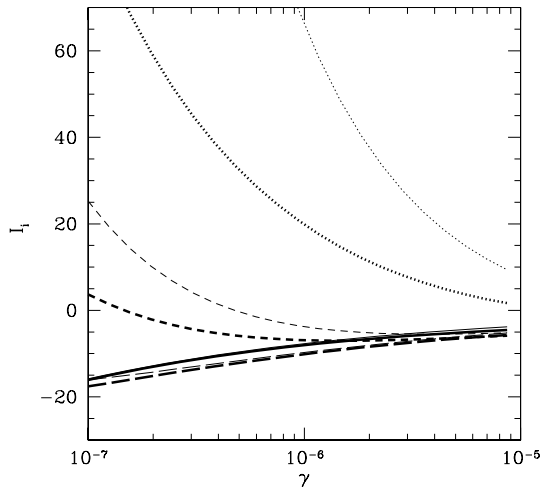

Figure 7. As Fig. 6, but for injection at line centre. Here the approximate versions include terms up to order β.

that carrying the series expansion to β^2 is quite accurate throughout the range $T_K \gtrsim 10$ K. In the injected case, the wing approximation is less useful because no analytic solution exits. Thus, we recommend numerical integration of equation (32) when high accuracy is required (especially at small temperatures).

6 SCATTERING OF Ly*n* PHOTONS

Consider a photon that redshifts into a Ly*n* line (with frequency ν_n) at redshift z_r; its frequency at redshift z is therefore $\nu_z = \nu_n[(1 + z)/(1 + z_r)]$. The accumulated optical depth it has traversed by that point is

$$\tau(z) = \int_z^\infty \mathrm{d}z \, \frac{\sigma(\nu_z) n_{\rm H\,I}(z) c}{(1+z) H(z)}, \tag{35}$$

where σ refers to the line of interest. The Gunn & Peterson (1965) optical depth is of course the *total* optical depth experienced by such a photon, or $\tau(z \ll z_r)$.

We are interested in determining the surface at which such a photon will *first* scatter. For the extremely optically thick Lyman-series lines of the IGM, this first scattering occurs far in the wings of the line, so we can set $\phi(x) \approx a/(\pi x^2)$. Further assuming the high-redshift limit [$H(z) \propto (1 + z)^{3/2}$] and letting $\Delta z \equiv z - z_r \ll z_r$, we have

$$\tau(z) \approx \frac{n_0^c \chi_n}{H_0 \sqrt{\Omega_0}} \, \frac{a}{\pi} \, \frac{(1+z_r)^{5/2}}{\Delta z \, \nu_n^2}, \tag{36}$$

where χ_n is evaluated for the line of interest. Re-expressing Δz in terms of x, we find

$$x(\tau) \approx \frac{1650}{\tau T_K^{1/2}} \left(\frac{\nu_\beta}{\nu_n}\right)^4 \left(\frac{A_n}{A_\beta}\right) \left(\frac{\Gamma_n}{\Gamma_\beta}\right) \left(\frac{1+z_r}{20}\right)^{3/2}, \tag{37}$$

where we have normalized ν_n, the spontaneous emission coefficients A_n and the inverse lifetimes Γ_n to the values appropriate for Lyβ. Higher Lyman-series photons have significantly longer lifetimes and

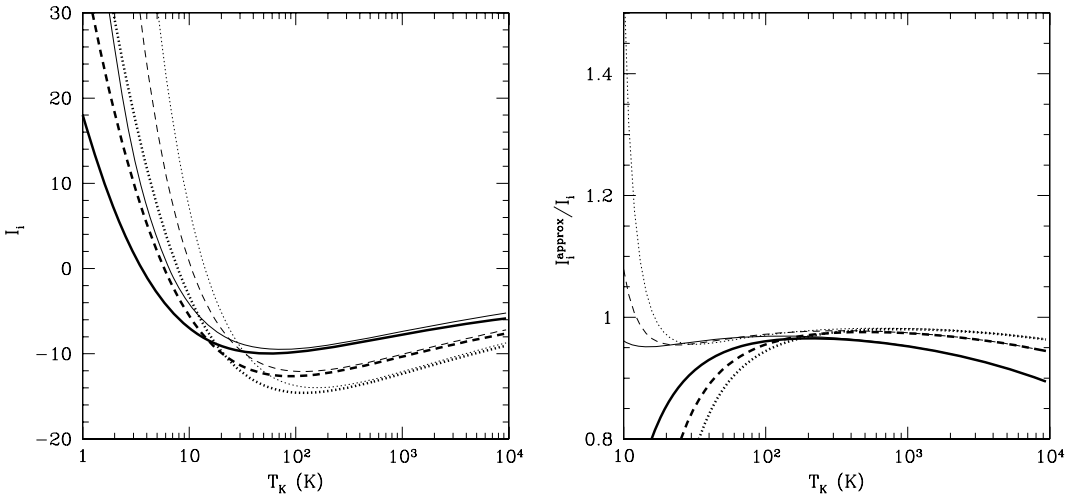

Figure 8. As Fig. 5, but for injection at line centre. In the right-hand panel, the approximate versions include terms up to order β (thick curves) and β^2 (thin curves).

hence scatter nearer line centre; for example, Lyϵ photons have a coefficient $\approx$18.

By setting $\tau = 1$ in equation (37), we see immediately that the first scattering occurs well blueward of resonance; we will denote this location x_1. Lyα photons cannot be destroyed during scattering (except, of course, in the exceedingly unlikely event that a collision occurs while the atom is excited), so this first scattering limit has little physical interest. However, higher Lyman-series photons can be destroyed, because the excited state can cascade to an intermediate level. The destruction probabilities per scattering are compiled by Hirata (2006) and Pritchard & Furlanetto (2006); they are $\sim$10 per cent for Lyβ and $\sim$20 per cent for higher-level transitions. Thus, each such photon scatters only a few times before vanishing; so long as they remain in the wings, the kth scattering will occur at $x_k \approx x_1/k$.

Because the photons are far out on the blue wing during each of these scattering events, they will deposit some fraction of their energy in the gas, heating it slightly. Our next goal is to calculate the net energy exchange with the IGM as these photons scatter and eventually disappear. We begin with the redistribution function $R_{\rm II}(x, x')$, which gives the probability that a photon absorbed at frequency x' is re-emitted at frequency x, assuming coherent scattering in the rest frame of the absorbing atom (Henyey 1941; Hummer 1962), thus ignoring recoil:

$$R_{\rm II}(x,x') = \frac{1}{\pi^{3/2}} \int_{|\overline{x}-\underline{x}|/2}^{\infty} {\rm d}u\, {\rm e}^{-u^2} \left[\tan^{-1}\left(\frac{\underline{x}+u}{a}\right) - \tan^{-1}\left(\frac{\overline{x}-u}{a}\right)\right], \quad (38)$$

where $\overline{x} = \max(x, x')$ and $\underline{x} = \min(x, x')$. This is normalized so that

$$\phi(x') = \int_{-\infty}^{\infty} {\rm d}x\, R_{\rm II}(x,x'). \quad (39)$$

In our case ($x' \gg 0$), the redistribution function is sharply peaked around x'. We thus write $x = x' + \Delta x$ and expand the inverse tangents to third order in $(u,\Delta x)$ about x' (note that, although u can be arbitrarily large, the exponential guarantees that only small values contribute to the integral). Equation (38) then becomes

$$R_{\rm II}(x,x') \approx \frac{a}{\pi^{3/2}x'^2} \int_{|\Delta x|/2}^{\infty} {\rm d}u\, {\rm e}^{-u^2} \left[(2u-\Delta x) + \frac{(\Delta x)^2 - 2u\Delta x}{x'}\right], \qquad x > x', \quad (40)$$

with a similar expression when $x < x'$. We are interested in the mean energy loss in each scattering,

$$\langle \Delta x | x' \rangle = \phi^{-1}(x') \int_{-\infty}^{\infty} {\rm d}x\, \Delta x\, R_{\rm II}(x,x'), \quad (41)$$

$$= \frac{-2}{\pi^{1/2}x'} \int_0^{\infty} {\rm d}\Delta x\, \Delta x^2 \times \int_{\Delta x/2}^{\infty} {\rm d}u\, {\rm e}^{-u^2}(2u-\Delta x), \quad (42)$$

where we have used the normalization of $R_{\rm II}$ and substituted our expansion for the redistribution function in the second equality. The integrals are elementary and are most easily performed by switching the order of integration; the simple result is

$$\langle \Delta x | x' \rangle = \frac{-1}{x'}. \quad (43)$$

This is identical to the second term in equation (3) of Chuzhoy & Shapiro (2006a) in the appropriate limit.

As expected, photons tend to lose energy to the gas, but only slowly. Physically, we have assumed that the scattering is coherent in the rest frame of the atom. Thus, in the IGM frame, the gas tends to gain energy if the scattering atom travels away from the initial photon and to lose energy if the atom travels towards it. When scattering occurs blueward of resonance, the former have a slightly higher cross-section for absorption because of the small blueshift imparted to them by their thermal velocity; thus the net effect is energy transfer to the gas. However, far out on the wings of the line, the difference in cross-sections from this displacement is small, and the heating is weak.

In contrast, consider scattering with zero natural width (or in other words where the total optical depth is small, so that the initial scattering occurs in the Doppler core). In that case, $R_{\rm II}$ simplifies to $R_{\rm I}(x, x') = {\rm erfc}(|\overline{x}|)/2$ (again assuming isotropic scattering in

the rest frame), where $\overline{|x|} = \max(|x|, |x'|)$ (Unno 1952). This has a flat core between $(-x', x')$, so the typical energy lost in the initial scattering is $\sim x'$. In this case, photons on the blue side are *only* scattered by atoms moving away from them (so that their frequency lines up with the infinitely sharp resonance), and in the lab frame the re-emitted photon typically shifts by a full Doppler width. Thus, in the few-scatterings limit, heating will be most efficient inside the line core. This is the case considered (for deuterium) by Chuzhoy & Shapiro (2006b).

Returning to the Ly*n* lines, where all the interactions occur in the wings, the net frequency shift in s scattering events is

$$\Delta x_{\rm tot} \approx \frac{s(1+s)}{2x_1}, \tag{44}$$

$$\sim 0.033 T_{\rm K}^{1/2} \left[\frac{s_n(1+s_n)}{110}\right] \left(\frac{\nu_n}{\nu_\beta}\right)^4 \left(\frac{A_\beta}{A_n}\right) \times \left(\frac{\Gamma_\beta}{\Gamma_n}\right) \left(\frac{1+z_{\rm r}}{20}\right)^{-3/2}. \tag{45}$$

Again, we have normalized to the values appropriate for Lyβ photons. Of course, we have assumed that the scatterings occur in the wings of the line. If the accumulated drift carries the photon towards line centre, subsequent scattering will occur symmetrically and heating will be negligible. Thus we must have $\Delta x_{\rm tot} \leqslant x_1$. This is marginally true for Lyϵ, which has $s_\epsilon = 5$ and a coefficient $0.77 T_{\rm K}^{1/2}$ when appropriate values are inserted into equation (45).

It is useful to compare this drift to that due to recoil itself, which we ignored by using $R_{\rm II}$. This has $\Delta x_{\rm recoil} = \eta$ per scattering. Thus

$$\frac{\Delta x_{\rm tot}}{\Delta x_{\rm recoil}} \sim 0.11 T_{\rm K} \left(\frac{1+s_n}{10}\right) \left(\frac{\nu_n}{\nu_\beta}\right)^4 \left(\frac{A_\beta}{A_n}\right) \left(\frac{\Gamma_\beta}{\Gamma_n}\right) \times \left(\frac{1+z_{\rm r}}{20}\right)^{-3/2}; \tag{46}$$

the coefficient is 2.35 for Lyϵ photons. Thus, at reasonably large temperatures, the frequency drift from repeated scattering overwhelms recoil. Pritchard & Furlanetto (2006) showed that recoil provides a negligibly small contribution at all temperatures. In practice, heating from Ly*n* scattering is never significant: only if $T_{\rm K} \gg T_\gamma$ could it possibly matter, but in that case other, much stronger, heating agents must already be present.

As we have shown, Δx is largest ($\sim$1) when scattering occurs near the line core. One example, considered by Chuzhoy & Shapiro (2006b), is the deuterium Lyβ resonance, for which the optical depth is of order unity. Then the energy transfer is much more efficient, and the temperature dependence differs. In either case, $\Delta T \propto h \Delta\nu_{\rm D} \langle \Delta x \rangle$ per scattering. When absorption is in the line centre $\langle \Delta x \rangle \sim 1$; in the wings, we have seen that natural broadening controls the cross-section and $\langle \Delta x \rangle \propto 1/x_1 \propto \Delta\nu_{\rm D}$. So $\Delta T_{\rm core} \propto T_{\rm K}^{1/2}$ and $\Delta T_{\rm wing} \propto T_{\rm K}$. Deuterium Ly$\beta$ turns out to be the most important transition (aside from hydrogen Lyα) in heat exchange and must be included in some circumstances. Of course, this energy is injected into the deuterium, rather than the hydrogen, to which it must be transferred by collisions. According to Chuzhoy & Shapiro (2006a), this is relatively inefficient. As a result, the deuterium temperature may become quite large ($T \sim 10^4$ K), where the wing approximation breaks down and the full Voigt profile must be used.

7 DISCUSSION

We have examined both analytic and numeric solutions for the radiation field near the Lyα resonance and used them to compute the total scattering rate and the IGM heating (or cooling) rate. We showed that the approximate analytic solution of Grachev (1989) and Chuzhoy & Shapiro (2006a), in which scattering in the wings dominates, is accurate so long as $T_{\rm K} \lesssim 1000$ K. At higher temperatures, thermal broadening becomes important. Fortunately, the scattering correction $S_\alpha \to 1$ at large temperatures. So the approximate fit presented by Chuzhoy & Shapiro (2006a) – our equation (21) – turns out to be reasonably accurate (to several per cent) whenever $T_{\rm K} \gtrsim 1$ K. For higher accuracy, equation (18) can be used.

We then used this analytic solution to examine the heating (or cooling) from the scattering near line centre. For the case of photons that redshift towards the resonance, we obtained a fully analytic solution (in terms of Airy functions) under the approximation that all scattering occurs in the wings. The arguments of the Airy functions are typically small, so a power series expansion is illuminating; it shows that the heating rate per atom and per Hubble time is proportional to $T_{\rm K}^{-1/3}(1+z)^{-2}$ when spin exchange can be neglected; this is an excellent approximation at $T_{\rm K} \gtrsim 10$ K. In the case of photons injected at line centre, we obtained a power series solution that converges reasonably rapidly. The lowest order term is reasonably accurate for $T_{\rm K} \gtrsim 100$ K, and in this regime the *cooling* rate per atom and per Hubble time is proportional to $T_{\rm K}^{1/3}(1+z)^{-5/2}$ (again when spin exchange can be neglected). Photons injected in this way only heat the gas when $T_{\rm K} \lesssim 10$ K.

Obviously, finding convenient and useful forms for S_α and the heating rates is a game of approximations. Because several different ones have been made in the literature, in Tables 1 and 2 we show the results for $(1 - S_\alpha)$ [essentially $\delta_J(0)$] and $I_{\rm c}$ in a variety of scenarios. The first row in each table gives our standard result (the thick curves in Figs 3 and 5), which includes the full Voigt profile and the detailed balance correction but ignores spin exchange and, of course, makes the Fokker–Planck approximation. The second row shows the results in the wing approximation of Grachev (1989) and Chuzhoy & Shapiro (2006a); it is excellent at low temperatures but begins to deviate by $\lesssim$10 per cent at higher temperatures where Voigt broadening is significant. The next row uses the approximate forms of equations (21) and (31); the latter is relatively poor at

Table 1. The quantity $(1 - S_\alpha)$ as a function of temperature $T_{\rm K}$ at $z = 20$ under several approximations (see text). Note that the fit in equation (21) was originally proposed by Chuzhoy & Shapiro (2006a).

Scenario	1 K	10 K	10^2 K	10^3 K	10^4 K
Normal	0.7798	0.3002	0.075 16	0.016 17	0.002 484
Wing approximation	0.7795	0.3001	0.075 27	0.016 57	0.003 175
Equation (21)	0.8175	0.3068	0.075 92	0.016 89	0.003 658
Detailed balance	0.7798	0.3003	0.075 28	0.016 29	0.003 137
Spin, $T_{\rm S} = T_\gamma$	0.7121	0.2956	0.075 46	0.016 29	0.002 511
Spin, $T_{\rm S} = T_{\rm K}$	0.8117	0.3034	0.075 25	0.016 18	0.002 484

Table 2. The quantity $I_{\rm c}$ as a function of temperature $T_{\rm K}$ at $z = 20$ under several approximations (see text).

Scenario	1 K	10 K	10^2 K	10^3 K	10^4 K
Normal	90.56	20.76	3.527	0.5346	0.069 40
Wing approximation	90.54	20.72	3.506	0.5243	0.065 58
First order (equation 31)	170.2	24.98	3.662	0.5293	0.065 69
Detailed balance	90.56	20.76	3.533	0.5437	0.083 46
Spin, $T_{\rm S} = T_\gamma$	88.99	20.70	3.546	0.5383	0.069 98
Spin, $T_{\rm S} = T_{\rm K}$	108.4	21.26	3.536	0.5347	0.069 40

small temperatures because it is only a first-order expansion. Next, we show the effects of ignoring the detailed balance correction: it also makes no difference at small temperatures, but it matters at the $\sim$15 per cent level at $T = 10^4$ K because the line broadening becomes relatively significant compared to the rest frequency of the line. In the next two lines, we show how including spin exchange affects the results. Because this introduces a new variable (T_S), we show the two limiting cases where $T_S = T_\gamma$ and $T_S = T_K$, which bracket the possible effects. Recall that this introduces a new source of drift and diffusivity, with a magnitude $\sim\nu_{21}^2/\Delta\nu_D^2$ (Hirata 2006; Chuzhoy & Shapiro 2006a). Thus it can make a substantial difference when $T_K \ll 10$ K, but for most of the range of interest its effects are small.

Finally, nearly all of the existing literature – including our calculations – uses the Fokker–Planck approximation, which assumes that the background spectrum is constant over the typical frequency change per scattering; as we have seen, this requires slow changes over $\Delta x \sim 1$ at line centre but is less restrictive in the wings. In general this is an excellent approximation; the background spectrum is in fact remarkably smooth (see Fig. 1). As emphasized by Hirata (2006), the worst-case scenario is for low-temperature gas (where the absorption trough is most sharply peaked) when spin diffusivity is included. Using a Monte Carlo model, he verified that the Fokker–Planck approximation for S_α is accurate to better than 3 per cent at $T_K = 2$ and 10 K, at a variety of spin temperatures. There have been no explicit tests at higher temperatures, and continued exploration of its accuracy is an important unsettled question. In fact, if this fractional uncertainty on S_α persists to higher temperatures, the fractional error on $1 - S_\alpha$ (and potentially I_c and I_i) could be huge at $T_K \gtrsim 1000$ K – even larger than those from the wing approximation. (Fortunately, of course, it is S_α itself – which is well-behaved – that is most important physically.) However (also as argued by Hirata 2006) the Fokker–Planck approximation is likely to be even more accurate in this high-temperature regime. First of all, the absorption feature becomes less pronounced so that the assumption that $J(\nu)$ is constant over the typical frequency change per scattering is more accurate. Secondly, spin effects become less significant, because the separate hyperfine lines become broadened into a single line. Meiksin (2006) also examined the Fokker–Planck approximation in the context of the heating rate, carrying the perturbative expansion to higher, post-diffusive order. Unfortunately, the resulting equations are not easy to manipulate or solve efficiently. In general, we expect the heating and cooling rates to be less sensitive to the Fokker–Planck assumption than S_α because most of the absorption feature appears at large x, where the frequency change per scattering is much less than unity and the smoothness requirement is less severe.

A final 'approximation' often made in the literature is to ignore Lyn photons. Their direct scattering contributes only $\lesssim 10^{-4}$ of the coupling (Pritchard & Furlanetto 2006) or $\lesssim 0.01$ of the heating (from the arguments in Section 6). However, $\sim$1/3 of these photons cascade to Lyα (Hirata 2006; Pritchard & Furlanetto 2006), which can have significant effects. For example, with Population II stars, $\sim$6 per cent of the total Lyα background comes from cascades. Because injected photons can cause cooling, even this small flux can qualitatively change the implications for T_K (Chuzhoy & Shapiro 2006b). They therefore cannot be ignored in this context.

As a final thought, it is useful to estimate the heating rate from Lyα scattering to gauge its importance relative to other processes. For simplicity, we will consider continuous injection (i.e. photons redshifting into the Lyα resonance). Inserting our lowest order approximation for I_c (from equation 31) into equation (26), we find

$$\frac{2}{3}\frac{\epsilon_\alpha}{H n_{H\,I} k_B T_K} \approx \frac{0.80}{T_K^{4/3}}\frac{x_\alpha}{S_\alpha}\left(\frac{10}{1+z}\right), \quad (47)$$

where the left-hand side is the fractional temperature change per Hubble time. On the right-hand side, we have rewritten $J(\nu)$ in terms of the 21-cm coupling efficiency x_α (see equation 15). The 21-cm spin temperature departs from the CMB temperature when $x_\alpha \sim 1$, so this is a convenient gauge for the background flux at which heating first becomes observationally relevant. Clearly, Lyα heating is negligible at this point unless the initial temperature is also small. (Note that this approximation for I_c *overestimates* the heating at low temperatures, so the actual coefficient is even smaller than predicted by equation 47.) Because, even without any heating, $T_K = 2.5$ K at $z = 10$ (Seager, Sasselov & Scott 1999), Lyα scattering is unlikely to be significant in this context: it alone will not suppress a 21-cm absorption epoch (Chen & Miralda-Escudé 2004).

Of course, the heating rate becomes much larger in strongly coupled gas. However, in practice it is still probably negligible compared to other processes such as X-ray heating (Oh 2001; Glover & Brand 2003; Furlanetto 2006). Following Furlanetto (2006), let us suppose that the X-ray emissivity traces the star formation rate (just like the Lyα emissivity). Then the ratio of X-ray and Lyα heating rates is

$$\frac{\epsilon_X}{\epsilon_\alpha} \sim 140 f_X T_K^{1/3}\left(\frac{f_{X,h}}{0.2}\frac{9690}{N_\alpha}\frac{1+z}{10}\right), \quad (48)$$

where we have again used our lowest order approximation to I_c and T_K is in Kelvin. Here $f_{X,h}$ is the fraction of X-ray energy that is used to heat the gas (Shull & van Steenberg 1985), N_α is the number of photons between Lyα and the Lyman-limit produced per baryon in stars (we have inserted the value appropriate for low-metallicity Pop II stars; Barkana & Loeb 2005), and f_X is the assumed X-ray luminosity per unit star formation calibrated to the local value between 0.2 and 10 keV (Ranalli, Comastri & Setti 2003; Gilfanov, Grimm & Sunyaev 2004). Clearly, Lyα heating is slow unless the X-ray emissivity is much smaller than its local value.

ACKNOWLEDGMENTS

We thank G. Rybicki and M. Furlanetto for helpful discussions.

REFERENCES

Barkana R., Loeb A., 2005, ApJ, 626, 1
Basko M. M., 1981, Astrophysics, 17, 69
Chen X., Miralda-Escudé J., 2004, ApJ, 602, 1
Chugai N. N., 1980, Sov. Astron. Lett., 6, 91
Chugai N. N., 1987, Astrofizika, 26, 89
Chuzhoy L., Shapiro P. R., 2006a, ApJ, submitted (astro-ph/0512206)
Chuzhoy L., Shapiro P. R., 2006b, ApJ, submitted (astro-ph/0604483)
Field G. B., 1958, Proc. I.R.E., 46, 240
Furlanetto S., 2006, MNRAS, 371, 867
Furlanetto S. R., Oh S. P., Briggs F. H., 2006, Phys. Rep. in press (astro-ph/0608032)
Gilfanov M., Grimm H.-J., Sunyaev R., 2004, MNRAS, 347, L57
Glover S. C. O., Brand P. W. J. L., 2003, MNRAS, 340, 210
Grachev S. I., 1989, Astrofizika, 30, 347
Gunn J. E., Peterson B. A., 1965, ApJ, 142, 1633
Henyey L. G., 1941, Proc. Nat. Acad. Sci., 26, 50
Hirata C. M., 2006, MNRAS, 367, 259
Hummer D. G., 1962, MNRAS, 125, 21
Hummer D. G., Rybicki G. B., 1992, ApJ, 387, 248

Madau P., Meiksin A., Rees M. J., 1997, ApJ, 475, 429
Meiksin A., 2006, MNRAS, 370, 2025
Oh S. P., 2001, ApJ, 553, 499
Pritchard J. R., Furlanetto S. R., 2006, MNRAS, 367, 1057
Ranalli P., Comastri A., Setti G., 2003, A&A, 399, 39
Rybicki G. B., 2006, ApJ, 647, 709
Rybicki G. B., dell'Antonio I. P., 1994, ApJ, 427, 603
Seager S., Sasselov D. D., Scott D., 1999, ApJ, 523, L1
Shull J. M., van Steenberg M. E., 1985, ApJ, 298, 268
Spergel D. N. et al., 2006, ApJ, submitted (astro-ph/0603449)
Unno W., 1952, PASJ, 3, 158
Wouthuysen S. A., 1952, AJ, 57, 31

This paper has been typeset from a TEX/LATEX file prepared by the author.